

Interference Cancellation for Coexistence of LoRaWAN With Wireless Power Transfer

Ryota Kumada¹ and Koichi Adachi¹, *Senior Member, IEEE*

Abstract—Low-power wide area networks (LPWANs), which realize long-distance communication with low-power consumption, are suitable for wireless sensor networks (WSNs). In particular, long-range wide area network (LoRaWAN) has been actively studied in recent years. Since wireless power transfer (WPT) charges the battery of terminals by sending high-frequency signals, it can avoid operational disruption for battery replacement and unnecessary wiring. However, if it is not well designed, WPT may cause interference to other wireless communication systems using the same frequency band. This article proposes a simple yet effective WPT interference cancellation method, which is suitable for LoRaWAN, to take a step to move the coexistence of LPWAN and WPT forward. The proposed method estimates the initial phase of the interfering signal by utilizing the packet frame structure of LoRaWAN and removes the interfering signal from the received signal during the signal detection process. Computer simulation results show that the proposed method can achieve almost the same symbol error rate (SER) performance as the system without interference, even under WPT interference.

Index Terms—Interference canceling, long-range wide area network (LoRaWAN), wireless power transfer (WPT), wireless sensor networks (WSNs).

I. INTRODUCTION

THE DEVELOPMENT of information and communication technology (ICT) has stimulated the rapid growth of Internet of Things (IoT) [1]. In the future, IoT networks will consist of billions of devices with various applications, such as smart metering and logistics tracking. Typical applications of IoT devices include large-scale wireless sensor networks (WSNs) that utilize information provided by many sensors, such as for environmental monitoring and production management [2]. These devices are required to operate with low-power consumption and be connected wirelessly to an aggregated information station, so various wireless communication protocols have been proposed. Low-power wide area networks (LPWANs) [3], including LoRa [4], Sigfox [5], and NB-IoT [6], enable low-power consumption and long-distance communication. In particular, chirp spread spectrum (CSS)-based LoRa modulation [7] achieves long-range communication by appropriately setting parameters, such as spreading

factor (SF) and coding rate. Thus, LoRa has attracted great interest as a communication protocol [8].

Due to the explosive growth of low-power devices, it is expected that wireless will be used not only information transmission but also energy supply in the future [9]. Wireless power transfer (WPT) solves the wiring problem, enables 24-h operation of factories, etc., since there is no need to shut down the device for battery replacement operations [10]. Furthermore, unlike energy harvesting, including solar power and thermoelectric power generation, WPT can provide highly reliable energy over the long term without depending on the surrounding environment. For this reason, WPT systems are being considered for future installation in smart factories and other facilities. When WPT systems operate at the same frequency as other wireless communication systems, the radio waves emitted by WPT cause co-channel interference (CCI) to other systems [11]. Therefore, it is necessary to consider the impact of CCI when multiple systems share the frequency spectrum.

A. Related Works

1) *Performance Evaluation of LoRaWAN*: The physical layer of LoRa is proprietary and patented by Semtech, but attempts to reverse engineering have revealed a mathematical description [7]. In addition, the bit error rate (BER) of the LoRa modulation has been evaluated under various channel conditions [13], [14]. It has been shown that LoRa modulation can exhibit high robustness of LoRa modulation against the channel conditions. On the other hand, it is known that the LoRa modulated signals with different SFs are not perfectly orthogonal [15], [16]. In [17], [18], and [19], it has been shown that collisions between nonorthogonal LoRa signals are destructive to the network capacity.

2) *Impact of CCI and Interference Cancellation*: In [20], the impact of interference on the LoRa modulation has been investigated when IEEE 802.15.4-g operates in the same frequency band. The results show that narrow bandwidths and smaller SFs, LoRa can achieve acceptable packet reception performance even if the interferer is about 6 [dB] stronger. If SF is larger than 9, the impact is negligible even when the interference signal power is higher than 16 [dB]. In [21], the impact of other communication protocols operating in the sub-GHz band (Sigfox, Z-wave, and IO Home Control) on LoRa has been evaluated. The results show that up to 20% of packet loss occurs if an interfering signal collides with the LoRa preamble and header. On the other hand, the interference

Manuscript received 29 June 2022; revised 3 November 2022 and 26 January 2023; accepted 13 March 2023. Date of publication 21 March 2023; date of current version 25 July 2023. This work was supported by JSPS KAKENHI under Grant JP22K04086. (Corresponding author: Koichi Adachi.)

The authors are with the Advanced Wireless and Communication Research Center, The University of Electro-Communications, Chofu 182-8585, Japan (e-mail: kumada@awcc.uec.ac.jp; adachi@awcc.uec.ac.jp).

Digital Object Identifier 10.1109/JIOT.2023.3259472

colliding with a payload does not almost impact the packet loss performance.

The impact of interference from various systems operating in the industrial, scientific, and medical (ISM) band on the BER performance of the LoRa modulation is evaluated in [22]. The effect of a frequency filter suppressing the interference from ultranarrowband signals, such as IEEE 802.15 on the BER performance is also evaluated. The results indicate that narrowband interference suppression is essential to maintain proper long-range wide area network (LoRaWAN) coverage. However, such a frequency filter suppresses the desired signal too. Thus, it concludes that a carefully designed SIR threshold should be introduced to avoid performance degradation.

Afisiadis et al. [23] evaluated the performance of the LoRa modulation schemes with coherent detection in the presence of LoRa signal interference using the same SF. They also derived exact approximations for symbol error rate (SER) and frame error rate (FER) performances. The coherent detection can provide up to 10 [dB] gain compared to the noncoherent detection. Several cancelation methods have been proposed to cancel interference between LoRa signals [24], [25], [26], [27], [28], [29]. In [25], a synchronization and successive interference cancelation (SIC) algorithm is proposed to decode superposed LoRa signals. This algorithm is applicable even when the transmitter and receiver are not time- and frequency-synchronized and the receiver receives multiple LoRa signals using the same SF simultaneously. This method reduces the number of packet retransmission and increases the network capacity.

3) *Impact of Interference From Wireless Power Transfer:* Since systems, such as LoRaWAN that operate in the unlicensed band or the ISM band share the same frequency band as the WPT system, there is concern that WPT interference may degrade their communication quality [22]. In [30], an analysis of the effect of continuous wave (CW) interference in orthogonal frequency division multiplexing (OFDM) systems is performed and an interference elimination method is proposed based on the results of the analysis. Interference rejection is achieved by estimating the CW parameters from the amount of interference added to two specific subcarriers and subtracting it from the original received signal. In [31], the impact of interference from WPTs on the LoRaWAN network has been analyzed in terms of communication performance degradation and network security. The communication performance has been shown to deteriorate as the number of WPT devices and transmission power increases, as well as the connectivity to network is degraded.

B. Objective and Contribution

Existing studies have shown that WPT interference degrades the performance of LoRaWAN. However, to the best of the authors' knowledge, how the WPT interference degrades the performance of LoRa systems has not been mathematically shown. Moreover, the WPT interference cancelation method at the LoRa receiver has not been proposed yet. Therefore, the purpose of this article is to realize the coexistence of LoRaWAN and WPT. First, we mathematically derive the

model how the WPT interference impacts on the LoRa detection. Then, we evaluate the impact of WPT interference on LoRaWAN. Second, we propose a simple WPT interference cancelation algorithm at the LoRa receiver. There are three major advantages of the proposed algorithm. First, it can be implemented in an existing LoRa receiver, and it does not require extra operations at the LoRa transmitter and energy transmitter (ET) sides. Second, it does not significantly affect the subsequent time-frequency synchronization algorithm because the proposed method works based on the preamble of the LoRa frame. Third, the algorithm is based entirely on a digital domain. Compared to interference suppression using conventional analog or digital filters [22], [32], the proposed algorithm does not distort the original signal component and does not affect LoRa symbol detection, which is a great advantage.

The proposed cancelation method operates as follows. The LoRa receiver first applies a LoRa-specific demodulation algorithm to the received signal. If the WPT interference exists, the interference signal is spread to all frequency bins by de-chirping. The LoRa receiver estimates the interference parameters by utilizing the frame preamble. Then, the receiver removes the interference in subsequent symbols based on the estimated parameters. After that, the symbols are demodulated based on the demodulation principles used in LoRa. Since the LoRa receiver performs parameter estimation only once per frame, the required computational complexity is slight. Furthermore, since the ET and the LoRa receiver are generally static, the change of the propagation parameters is also relatively slow. Thus, the LoRa receiver can use the estimated parameters to demodulate the whole LoRa symbols within a frame. Computer simulations confirm that the proposed method can remove WPT interference and reduce the performance degradation of LoRaWAN. The proposed method is also shown to be effective in more realistic environments.

The contributions of this study can be summarized as follows.

- 1) We show the received signal model at the LoRa receiver in the presence of WPT interference signals and evaluate the degradation of LoRa performance due to WPT interference.
- 2) We propose a simple yet effective interference cancelation algorithm. The algorithm is implemented only in the LoRa receiver and does not require any information of the interfering signal.
- 3) We evaluate the proposed interference cancelation algorithm by computer simulation and show the effectiveness of the proposed method. Furthermore, we confirm that the proposed method can be applied in a more realistic environment.

C. Organization

The remainder of this article is organized as follows. Section II provides an overview of LoRa modulation schemes. Section III presents the WPT model, its interference model, and an evaluation of LoRa system performance in the presence of WPT interference. Section IV presents the proposed

TABLE I
NOTATIONS AND DEFINITIONS

Notation	Definitions
S	Spreading factor
T_c	Chip length [sec]
$T_s = 2^S \times T_c$	Symbol length [sec]
$W = 1/T_c$	Bandwidth [Hz]
$\mathcal{M} = \{0, 1, \dots, 2^S - 1\}$	Set of symbols
$x \bmod a$	Modulo a operation of x
j	Imaginary unit
$(\cdot)^*$	Complex conjugate
$(\cdot)^T$	Transpose operation
\otimes	Convolution operation
$\mathbb{E}[\cdot]$	Ensemble average
$\mathcal{F}[\cdot]$	Discrete Fourier transform
$\Re[\cdot]$	Real part of the argument
$\delta(\cdot)$	Delta function
$\mathcal{CN}(\mu, \sigma^2)$	The distribution of a circularly symmetric complex Gaussian (CSCG) random variable with mean μ and variance σ^2

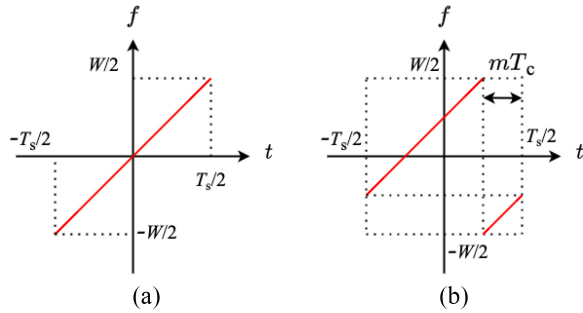


Fig. 1. LoRa signals. (a) Raw up-chirp signal ($m = 0$). (b) Cyclic shift mT_c corresponding to symbol m .

WPT interference rejection algorithm for LoRa receivers and its principle of operation, followed by an evaluation based on computer simulations in Section V. Finally, Section VI concludes this article.

II. OVERVIEW OF LoRa MODULATION

This section describes the CSS modulation used in the physical (PHY: Physical) layer of LoRaWAN [7]. In this article, we use the notations and definitions given in Table I.

One of the key parameters in CSS modulation is the SF, which represents the number of bits transmitted by one CSS symbol. LoRaWAN can cover a wide communication area by setting SF appropriately for the communication environment.

A. Chirp Spread Spectrum Modulation

In CSS modulation, the signal is spread by varying the signal frequency over time within a frequency band. By sampling at $T_c = 1/W$ [sec] intervals, the k th chip of the reference CSS modulated baseband signal [Fig. 1(a)] can be expressed as

$$\begin{aligned} x_0[k] &= \frac{1}{\sqrt{2^S}} \exp\left(j2\pi \cdot \frac{(kT_c)^2 W}{2T_s}\right) \\ &= \frac{1}{\sqrt{2^S}} \exp\left(j2\pi \cdot \frac{k^2}{2^{S+1}}\right) \end{aligned} \quad (1)$$

where $T_s = 2^S \cdot T_c$ and $W = 1/T_c$. One CSS symbol consists of 2^S chips and represents S information bits by cyclically shifting reference CSS modulated signal. Thus, as shown in Fig. 1(b), symbol $m \in \mathcal{M}$ is equivalent to cyclically delaying chirp signal $x_0[k]$ by mT_c [sec] and can be represented by

$$x_m[k] = \frac{1}{\sqrt{2^S}} \exp\left(j2\pi \cdot \frac{((k+m) \bmod 2^S)^2}{2^{S+1}}\right). \quad (2)$$

The chirp signal, $x_m[k]$, also represents the 2^S orthonormal basis functions that construct the multidimensional space of the LoRa signal.

B. Demodulation of LoRa Signal

In this section, we describe a mathematical model and demodulation principle of LoRa received signals. We consider a discrete-time multipath fading channel defined as

$$g[k] = \sum_{\ell=0}^{L^{\text{CSS}}-1} g_\ell \delta(k - \tau_\ell^{\text{CSS}}) \quad (3)$$

where L^{CSS} is the number of multipaths for the LoRa signal, g_ℓ and τ_ℓ^{CSS} are the complex path coefficient and time delay of the ℓ th path, respectively. We assume the block fading channel, i.e., $g[k]$ keeps invariant within a LoRa PHY frame. Due to the narrowband transmission, the symbol length of one CSS symbol is significantly longer than the possible path delays and, hence, we assume that inter symbol interference (ISI) only occurs from the previous symbol to the current symbols [19]. Thus, the symbols in a receive window can be written as follows:

$$\tilde{m}_\ell \triangleq \begin{cases} \tilde{m}, & \text{for } k = 0, \dots, \tau_\ell^{\text{CSS}} - 1 \text{ (previous symbol)} \\ m, & \text{for } k = \tau_\ell^{\text{CSS}}, \dots, 2^S - 1 \text{ (current symbol)}. \end{cases} \quad (4)$$

In this case, the signals corresponding to previous/current symbol can be expressed as follows:

$$x_{\tilde{m}_\ell}[k - \tau_\ell^{\text{CSS}}] = \begin{cases} x_{\tilde{m}}[2^S - \tau_\ell^{\text{CSS}} + k], & \text{for } k = 0, \dots, \tau_\ell^{\text{CSS}} - 1 \\ x_m[k - \tau_\ell^{\text{CSS}}], & \text{for } k = \tau_\ell^{\text{CSS}}, \dots, 2^S - 1. \end{cases} \quad (5)$$

Assuming perfect time-frequency synchronization for the first path (i.e., $\tau_0^{\text{CSS}} = 0$), the received signal is given by

$$y[k] = \sqrt{\frac{E_s}{T_c}} g[k] \otimes x_m[k] + \sum_{m'=0}^{2^S-1} w_{m'} x_{m'}[k] \quad (6)$$

where E_s is the energy per CSS symbol, $w_{m'}$ is the AWGN following $\mathcal{CN}(0, \sigma_w^2)$ within the m' th dimension of LoRa signal [33]. The demodulation process of this LoRa signal can be easily implemented by the following steps [34].

1) *Dechirping With Reference Down Chirp Signals*: The k th chip element obtained by multiplying the received signal by the reference downchirp signal $x_0^*[k]$.

2) *Discrete Fourier Transform*: A 2^S -point discrete Fourier transform (DFT) is performed on the output chip sequence after dechirping. The n th frequency bin of the DFT output is given by

$$R(n) = \mathcal{F} \left[\underbrace{y[k]x_0^*[k]}_{\text{dechirping}} \right] = \sum_{k=0}^{2^S-1} (y[k]x_0^*[k]) \exp\left(-j2\pi \frac{n}{2^S}k\right). \quad (7)$$

Then, the DFT output of the LoRa signal can be written as follows:

$$\sum_{k=0}^{2^S-1} \{(g[k] \otimes x[k])x_0^*[k]\} \exp\left(-j2\pi \frac{n}{2^S}k\right) = \sum_{\ell=0}^{L^{\text{css}}-1} \tilde{g}_{\tilde{m}_\ell}(\tau_\ell^{\text{css}}) \left\{ \frac{1}{2^S} \sum_{k=0}^{2^S-1} \exp\left(j2\pi \frac{\tilde{m}_\ell - \tau_\ell^{\text{css}} - n}{2^S}k\right) \right\} \quad (8)$$

where $\tilde{g}_{\tilde{m}_\ell}(\tau_\ell^{\text{css}}) = g_\ell \exp(j2\pi[(\tilde{m}_\ell - \tau_\ell^{\text{css}})^2]/2^{S+1})$ is the ℓ th equivalent path coefficient.

Proof: See the Appendix. ■

Consequently, each frequency bin of the DFT output becomes as

$$R(n) = \sqrt{\frac{E_s}{T_c}} \sum_{\ell=0}^{L^{\text{css}}-1} \tilde{g}_{\tilde{m}_\ell}(\tau_\ell^{\text{css}}) \times \left\{ \frac{1}{2^S} \sum_{k=0}^{2^S-1} \exp\left(j2\pi \frac{\tilde{m}_\ell - \tau_\ell^{\text{css}} - n}{2^S}k\right) \right\} + \exp\left(j2\pi \frac{n^2}{2^{S+1}}\right) w_n. \quad (9)$$

In particular, for $L^{\text{css}} = 1$, (9) can be simplified as

$$R(n) = \sqrt{\frac{E_s}{T_c}} \tilde{g}_m(0) \delta(m-n) + \exp\left(j2\pi \frac{n^2}{2^{S+1}}\right) w_n. \quad (10)$$

Equation (10) indicates that only the frequency bin corresponding to the transmitted m th symbol has a signal component, and the other bins have only noise component. There are two types of symbol detection, coherent and noncoherent. In general, noncoherent detection is used because coherent detection requires channel estimation and compensation, which increases the complexity of a receiver. In noncoherent detection, the transmitted symbols can be easily detected by taking the magnitude of DFT output $R(n)$. The symbol detection is expressed as

$$m^* = \underset{m' \in \mathcal{M}}{\operatorname{argmax}} (|R(m')|). \quad (11)$$

Fig. 2(a) shows an example of the DFT output given by (10) with the signal-to-noise power ratio (SNR) $\gamma_{\text{SNR}} = E_s/(2^S \cdot N_0) = -2.0$ dB (N_0 is the one-sided power spectrum density of the noise) for a transmit symbol of $m = 30$. As can be seen from this figure, a peak appears at the $m = 30$ th frequency index. The CSS modulation is known to be robust to noise and interference because it provides a processing gain of 2^S .

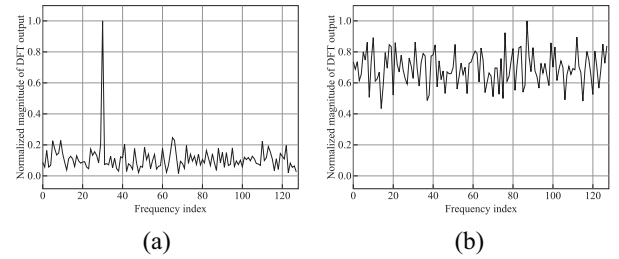


Fig. 2. Example of DFT output with $S = 7$ and $W = 125$ [kHz]. (a) Interference free. (b) With WPT interference $\varepsilon = 0$.

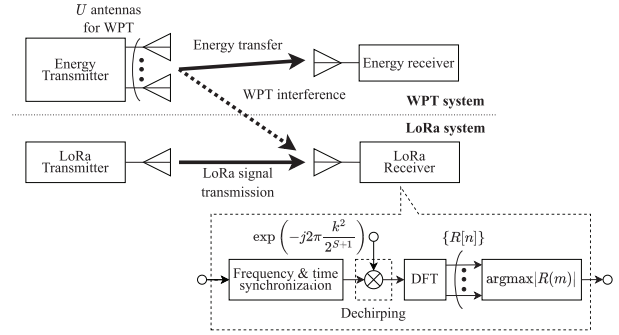


Fig. 3. System model and LoRa receiver block diagram.

III. WIRELESS POWER TRANSFER

This section details the WPT signal model and presents the interference model at the LoRa receiver. This article assumes that the WPT system and the LoRa system are different systems, where the WPT system is dedicated to power transfer. Therefore, all WPT signals at the LoRa receiver are treated as interference, as shown in Fig. 3.

A. Signal and System Model

Consider a system in which an ET with U antennas transmits energy to energy receivers in a typical multipath environment. The ET may transmit multiple unmodulated sine waveforms over multiple frequencies to boost power transfer efficiency [35], [36]. The frequencies are evenly spaced by intercarrier frequency spacing Δ_f . Since frequency spacing Δ_f is generally wider than the bandwidth of LoRa W [37], [38], in the following, we will assume a single sine wave with carrier frequency f_c^{wpt} [Hz] exists within the LoRa signal bandwidth. With the above assumptions, the bandpass signal transmitted by ET is given by

$$\mathbf{x}_{\text{RF}}^{\text{wpt}}(t) = \Re[\mathbf{x} \cdot \exp(j2\pi f_c^{\text{wpt}} t)] \quad (12)$$

where $\mathbf{x} \triangleq [x_1, \dots, x_U]^T$ is the weight vector whose element is given by $x_u = s_u^{\text{wpt}} \exp(j\phi_u^{\text{wpt}})$. s_u^{wpt} and ϕ_u^{wpt} denote the amplitude and phase of the sine wave transmitted by the antenna u , respectively.

The WPT signal propagates through the L^{wpt} multipaths [39] and arrives at the LoRa receiver. Let $\tau_{\ell,u}^{\text{wpt}}$, $\alpha_{\ell,u}$, and $\xi_{\ell,u}$ denote the distinct delay, amplitude gain, and phase shift of path ℓ . Let $\Delta_{\ell,u}(t) = 2\pi f_c^{\text{wpt}}(t - \tau_{\ell,u}^{\text{wpt}}) + \xi_{\ell,u}$, the received signal can

be expressed as

$$\begin{aligned} y_{\text{RF}}^{\text{wpt}}(t) &= \Re \left[\sum_{u=0}^{U-1} \sum_{\ell=0}^{L-1} \alpha_{\ell,u} x_u \exp(j\Delta_{\ell,u}(t)) \right] + w(t) \\ &= \Re [\mathbf{h}\mathbf{x} \cdot \exp(j2\pi f_c^{\text{wpt}} t)] + w(t) \end{aligned} \quad (13)$$

where $\mathbf{h} \triangleq [h_1, \dots, h_U]$ denotes the channel vector and $h_u = \sum_{\ell=0}^{L-1} a_{\ell,u} \exp(j(-2\pi f_c^{\text{wpt}} \tau_{\ell,u} + \xi_{\ell,u}))$. In the following, we consider the case with $L^{\text{wpt}} = 1$ only for simplicity. The rationale behind this assumption is that the unmodulated sine wave transmitted from each antenna becomes a constant phase sine wave when it is received at the antenna propagating through multiple paths.

B. Impact of WPT on LoRaWAN

This section describes the reception model of WPT interference signals at LoRa receivers. From (12), the baseband WPT interference signal at time t can be expressed as

$$\mathbf{x}^{\text{wpt}}(t) = \mathbf{x} \exp(j2\pi f^{\text{off}} t) \quad (14)$$

where f^{off} represents the offset between carrier frequency f_c^{css} used for LoRa signals and the one used for WPT f_c^{wpt} . The discrete-time representation of $\mathbf{x}^{\text{wpt}}(t)$ is given as

$$\begin{aligned} \mathbf{x}^{\text{wpt}}[k] &= \mathbf{x} \exp\left(j2\pi \frac{f^{\text{off}}}{W} k\right) \\ &= \mathbf{x} \exp(j2\pi \varepsilon k). \end{aligned} \quad (15)$$

For notational convenience, let $\varepsilon \triangleq f^{\text{off}}/W$ denote the frequency offset f^{off} normalized by the LoRa signal bandwidth W . The received signal at the LoRa receiver in the existence of WPT interference can be expressed as follows:

$$y[k] = \sqrt{\frac{E_s}{T_c}} g[k] \otimes x_m[k] + \sum_{m'=0}^{2^S-1} w_{m'} x_{m'}[k] + \mathbf{h}\mathbf{x}^{\text{wpt}}[k]. \quad (16)$$

In the simulation results, we will evaluate the impact of channel time selectivity. The LoRa receiver detects the transmitted symbols as described in Section II-B. The interference signal, $x^{\text{wpt}}[k]$, at the k th sampling time, obtained by multiplying the received signal by the downchirp, is

$$\begin{aligned} \mathbf{h}\mathbf{x}^{\text{wpt}}[k] x_0^*[k] &= \underbrace{\mathbf{h}\mathbf{x}}_{\triangleq \sqrt{P_{\text{int}}} \exp(j\varphi_{\text{int}})} \exp(j2\pi \varepsilon k) \\ &\quad \times \frac{1}{\sqrt{2^S}} \exp\left(-j2\pi \frac{k^2}{2^{S+1}}\right) \\ &= \sqrt{\frac{P_{\text{int}}}{2^S}} \exp\left(j2\pi \left(\varepsilon k - \frac{k^2}{2^{S+1}} + \varphi_{\text{int}}\right)\right) \end{aligned} \quad (17)$$

where $P_{\text{int}} = \mathbb{E}[|\mathbf{h}\mathbf{x}|^2]$ represents the interference signal power and $\varphi_{\text{int}} \in [0; 2\pi)$ denotes the phase of the interfering signal. The interference in the n th symbol component obtained by

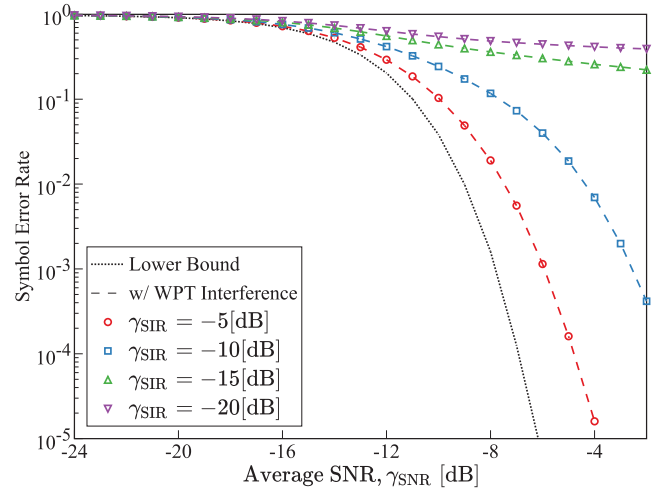


Fig. 4. Average SER performance under WPT interference with $S = 7$, $W = 125$ [kHz], and $\varepsilon = 0$.

applying DFT to the down-chirped output chip sequence is given by

$$\begin{aligned} R^{\text{wpt}}(n) &= \mathcal{F}[\mathbf{h}\mathbf{x}^{\text{wpt}}[k] x_0^*[k]] \\ &= \sum_{k=0}^{2^S-1} (\mathbf{h}\mathbf{x}^{\text{wpt}}[k] x_0^*[k]) \times \exp\left(-j2\pi \frac{n}{2^S} k\right) \\ &= \sqrt{P_{\text{int}}} \exp(j\varphi_{\text{int}}) \\ &\quad \times \underbrace{\frac{1}{\sqrt{2^S}} \sum_{k=0}^{2^S-1} \exp\left(j2\pi \left(\varepsilon k - \frac{k^2}{2^{S+1}} - \frac{n}{2^S} k\right)\right)}_{\triangleq z(\varepsilon, n)} \\ &= \sqrt{P_{\text{int}}} \exp(j\varphi_{\text{int}}) \cdot z(\varepsilon, n) \end{aligned} \quad (18)$$

where $z(\varepsilon, n)$ is a complex function that is uniquely determined from frequency offset ε normalized by the bandwidth of the LoRa signal. Therefore, the DFT output of the LoRa receiver in the presence of interfering signals due to WPT can be summarized as (19), shown at the bottom of the page.

The LoRa receiver detects the transmitted symbol based on (11), which implies that the WPT interference signal affects the symbol detection. Fig. 2(b) shows an example of DFT output (19) when $\gamma_{\text{SNR}} = -2.0$ [dB], $\text{SIR } \gamma_{\text{SIR}} \triangleq P_s/P_{\text{int}} = -15.0$ [dB] with $m = 30$, where P_s is the desired signal power and $P_s = E_s/T_s$. Thus, the desired signal component is buried in the interference component, and a symbol detection error occurs because the maximum value is taken at a frequency bin different from the transmitted symbol. In general, the transmit power used for WPT is higher than that for LoRa signals, so the impact of WPT interference cannot be ignored when LoRa and WPT systems are implemented in the same environment. Fig. 4 shows the SER performance of the LoRa signal in the existence of WPT interference. The

$$R(n) = \sqrt{\frac{E_s}{T_c}} \sum_{\ell=0}^{L^{\text{css}}-1} \tilde{g}_{\tilde{m}_\ell}(\tau_\ell) \left\{ \frac{1}{2^S} \sum_{k=0}^{2^S-1} \exp\left(j2\pi \frac{\tilde{m}_\ell - \tau_\ell - n}{2^S} k\right) \right\} + \exp\left(j2\pi \frac{n^2}{2^{S+1}}\right) w_n + \sqrt{P_{\text{int}}} \exp(j\varphi_{\text{int}}) \cdot z(\varepsilon, n) \quad (19)$$

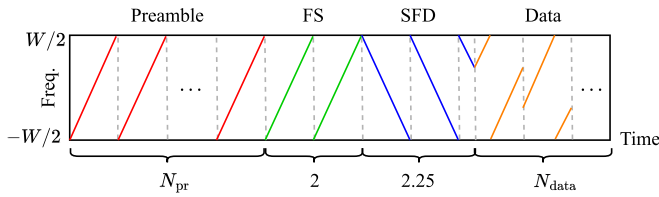


Fig. 5. Uplink LoRa frame structure [40].

SF is $S = 7$, the bandwidth $W = 125$ [kHz], and the normalized carrier frequency offset between the LoRa signal and WPT is $\varepsilon = 0$. As can be seen from the figure, although the effect of interference becomes smaller as the SIR increases, the SER performance significantly degrades compared to the case without WPT interference.

IV. PROPOSED WPT CANCELLATION

This section describes the operation of the proposed interference cancellation method that can effectively remove interfering WPT signals. The proposed method requires information that can be estimated at the receiver and requires no additional processing at the ET or LoRa transmitter. As (19) shows, the unknown parameters required for eliminating interference are normalized frequency offset ε , initial phase φ_{int} , and power P_{int} of interference signal. As shown in Fig. 2(b), the interference power contained in the m th frequency bin may cancel out the LoRa signal power, which results in misdetection of the LoRa signal. Therefore, we focus on the frame structure of the LoRaWAN, which is shown in [40, Fig. 5].

Fig. 6 shows an overview of the proposed method. The process of the proposed method is as follows. Once the LoRa receiver detects a preamble, it estimates the parameters of the interference signal in a frequency domain. Then, the receiver performs interference cancellation for subsequent symbols in the frequency domain based on the estimated parameters. Please note that the proposed method does not require channel state information \mathbf{h} of WPT signal. Finally, the receiver demodulates the symbols using the conventional LoRa demodulation algorithm. Fig. 7 is the flowchart of the proposed interference cancellation method. The proposed method is composed of the following four steps.

- 1) Normalized frequency offset ε estimation of interference WPT signal
- 2) Initial phase φ_{int} and power P_{int} estimation of interfering WPT signal
- 3) Interference signal cancelation based on the estimated parameter
- 4) Transmitted symbol detection from the interference eliminated signals

A. Frequency Offset Estimation of Interference Signal

In this section, we show how to estimate normalized frequency offset ε . Note that the receiver needs to carry out this frequency offset estimation only once when the system turns on as long as the ET does not change the carrier frequency. Since $z(\varepsilon, n)$ in (18) is a complex value, we can write it in

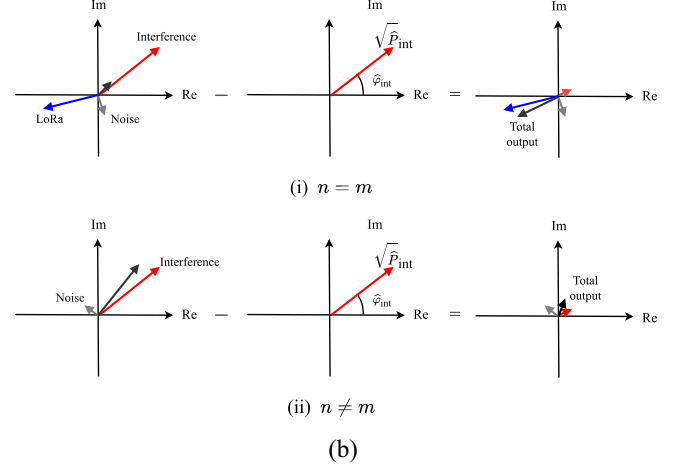
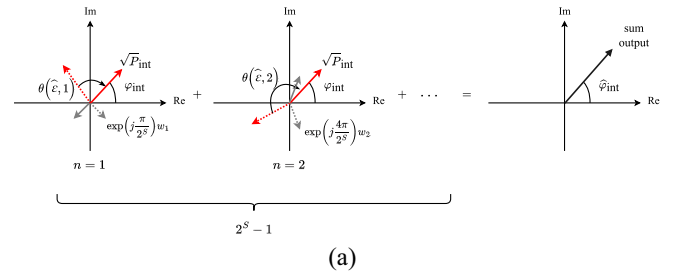


Fig. 6. Overview of proposed interference cancellation method. (a) Parameter estimation. (b) WPT interference cancellation.

the polar form as $z(\varepsilon, n) = r(\varepsilon, n) \cdot \exp(j\theta(\varepsilon, n))$. In addition, because symbols are sent consecutively in a frame, a phase offset $\psi^{\text{pr}}(\varepsilon, p) = 2\pi\varepsilon p T_s \bmod 2\pi$ is added when the p th preamble symbol is received. We project the frequency bins except for $n = 0$ to different $\exp(-j(\theta(\varepsilon', n) + \psi^{\text{pr}}(\varepsilon', p)))$ and estimate $\hat{\varepsilon}$ that shows the maximum absolute value as follows:

$$\hat{\varepsilon} = \operatorname{argmax}_{\varepsilon' \in \mathcal{U}} \left| \sum_{p=i_{\text{pr}}}^{N_{\text{pr}}-1} \sum_{n=1}^{2^S-1} C_p(\varepsilon', n) \right| \quad (20)$$

where $C_p(\varepsilon', n) = R_p(n) \exp(-j(\theta(\varepsilon', n) + \psi^{\text{pr}}(\varepsilon', p)))$ is the correlation like values obtained by projection. $\mathcal{U} = \{-0.5, -0.5 + \Delta_\varepsilon, -0.5 + 2\Delta_\varepsilon, \dots, 0.5 - \Delta_\varepsilon, 0.5\}$ is the set of normalized frequency offset candidates with Δ_ε being the search step size and N_{pr} is preamble length. i_{pr} is the starting index of the detected preambles. $R_p(n)$ is n th frequency bin at the p th preamble symbol. The reason for omitting the $n = 0$ th frequency bin from the summation is that the estimation accuracy can be improved by excluding the $n = 0$ th frequency bin that contains the reference up chirp signal (preamble signal) propagating through the $\ell = 0$ th path. If the previous LoRa symbol and the current one have the same chirp index n , the DFT output (9) has peaks at $((n - \tau_\ell^{\text{css}}) \bmod 2^S)$ th frequency bins, which is the case for the preamble part with $n = 0$. Thus, even for the preamble signal with $n = 0$, the DFT output has L^{css} peaks. However, it is difficult to know the positions of those peaks at the receiver because the LoRa receiver does not perform any channel estimation. However, the impact of

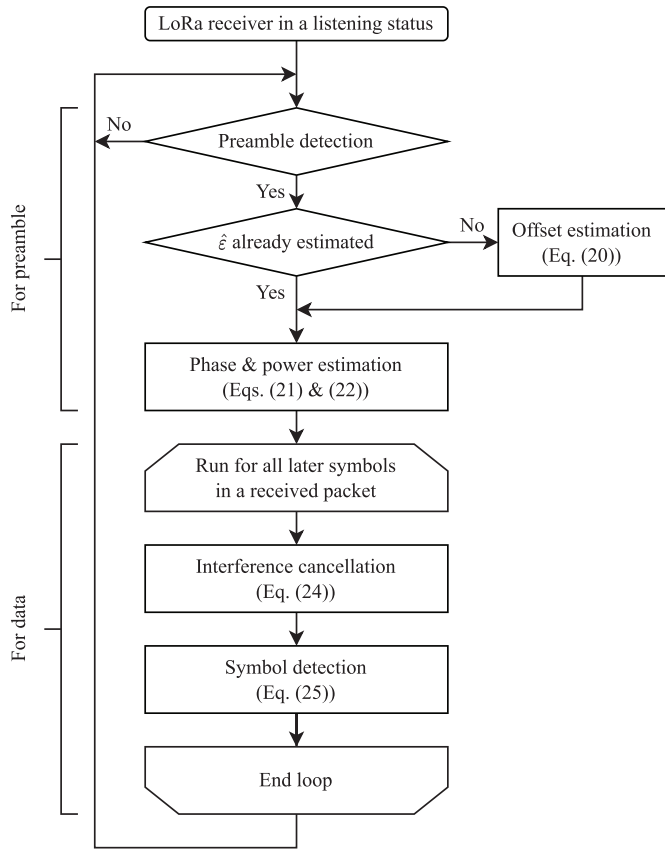


Fig. 7. Flowchart of the proposed interference cancellation method.

those peaks on the estimation accuracy of the proposed method is marginal due to the following reasons.

- 1) Generally, the delay path is weaker than the first path, i.e., the amplitude of signal on those $L^{\text{CSS}} - 1$ peaks is relatively small.
- 2) The WPT interference is enhanced due to summation as its frequency components are in phase.

Thus, the impact of the preamble signal propagating through the delayed paths is negligible.

B. Initial Phase and Power Estimation of Interference Signal

Once the normalized frequency offset is estimated, the next step is to estimate initial phase φ_{int} and power P_{int} of the interfering signal. As (18) indicates, the LoRa receiver can

calculate phase rotation $\theta(\epsilon, n)$ of the interference component added to each frequency bin. Therefore, as shown in Fig. 6(a), we compensate for phase rotation $\theta(\hat{\epsilon}, n)$ introduced to each frequency bin and calculate the argument for the sum of the frequency bins except for the $n = 0$ th. The reason for excluding $n = 0$ th is, same as in the previous section, to improve estimation accuracy. From the above, an initial phase φ_{int} of the WPT interference can be estimated as (21), shown at the bottom of the page, where I^{CSS} is the LoRa multipath component.

Similarly, the interfering signal power can be estimated as

$$\hat{P}_{\text{int}} = \frac{\left| \sum_{n=1}^{2^S-1} R(n) \cdot \exp(-j\theta(\hat{\epsilon}, n)) \right|^2}{\left(\sum_{n=1}^{2^S-1} r(\hat{\epsilon}, n) \right)^2} \stackrel{(a)}{\approx} \frac{\left| I^{\text{CSS}} + \exp(j\varphi_{\text{int}}) \cdot \sqrt{P_{\text{int}}} \sum_{n=1}^{2^S-1} r(\hat{\epsilon}, n) \right|^2}{\sum_{n=1}^{2^S-1} r(\hat{\epsilon}, n)^2} \quad (22)$$

where (a) is due to the following fact that the noise component $\{w_n\}$ is i.i.d and they can sufficiently cancel out each other by summation

$$\sum_{n=1}^{2^S-1} \left(\exp\left(j2\pi \frac{n^2}{2^{S+1}} k\right) w_n \cdot \exp(-j\theta(\hat{\epsilon}, n)) \right) \approx 0. \quad (23)$$

C. WPT Interference Cancellation

Once the interfering signal phase and power are estimated, the interference components are removed from the DFT output. For each frequency bin of the DFT output in the q th payload symbol, the interference is removed based on the estimated parameters as follows:

$$R'_q(n) = R_q(n) - \sqrt{\hat{P}_{\text{int}}} \exp\left(j\left(\hat{\varphi}_{\text{int}} + \psi^{\text{pl}}(\hat{\epsilon}, q)\right)\right) \cdot z(\hat{\epsilon}, n) \quad (24)$$

where $\psi^{\text{pl}}(\hat{\epsilon}, q) = 2\pi \hat{\epsilon} (N_{\text{pr}} + N_{\text{FS}} + N_{\text{SFD}} + q) T_s \bmod 2\pi$ is the phase offset at the q th payload symbol. N_{FS} and N_{SFD} are Frequency Sync. and Start Frame Delimiter length, respectively. Thus, $R'(n)$ has noise and residual interference due to imperfect parameter estimation. In addition, only one frequency bin $n = m$, i.e., $R'(m)$, has a LoRa signal energy.

$$\begin{aligned} \hat{\varphi}_{\text{int}} &= \arg \left(\sum_{n=1}^{2^S-1} R(n) \cdot \underbrace{\exp(-j\theta(\hat{\epsilon}, n))}_{\text{phase compensation}} \right) \\ &= \arg \left(\underbrace{\sum_{n=1}^{2^S-1} \sqrt{\frac{E_s}{T_c}} \sum_{\ell=0}^{L^{\text{LoRa}}-1} \tilde{g}_{m_\ell}(\tau_\ell) \left\{ \frac{1}{2^S} \sum_{k=0}^{2^S-1} \exp\left(j2\pi \frac{\tilde{m}_\ell - \tau_\ell - n}{2^S} k\right) \right\}}_{\triangleq I^{\text{CSS}}} \cdot \exp(-j\theta(\hat{\epsilon}, n)) \right. \\ &\quad \left. + \underbrace{\sum_{n=1}^{2^S-1} \exp\left(j2\pi \frac{n^2}{2^{S+1}}\right) w_n \cdot \exp(-j\theta(\hat{\epsilon}, n))}_{\approx 0} + \sum_{n=1}^{2^S-1} \sqrt{P_{\text{int}}} \exp(j\varphi_{\text{int}}) \cdot r(\hat{\epsilon}, n) \right) \approx \arg \left(I^{\text{CSS}} + \exp(j\varphi_{\text{int}}) \cdot \underbrace{\sqrt{P_{\text{int}}} \sum_{n=1}^{2^S-1} r(\hat{\epsilon}, n)}_{\text{Real value}} \right) \quad (21) \end{aligned}$$

TABLE II
REQUIRED NUMBER OF COMPLEX MULTIPLICATIONS FOR THE PROPOSED METHOD

Operation	Value
Normalized frequency offset ε estimation	$\frac{1}{\Delta_\varepsilon} \cdot ((2^S - 1) + (N_{\text{pr}} - i_{\text{pr}})(2^S - 1))$
Phase φ_{int} estimation	$2^S - 1$
Power P_{int} estimation	$2 \cdot (2^S - 1) + 1$
Interference cancellation	$N_{\text{pl}} \cdot 2^S$

D. Symbol Detection

For the n th frequency bin after interference cancelation, the LoRa receiver consider that the m^* th symbol with the maximum absolute value to be the transmitted symbol, i.e.,

$$m^* = \underset{m' \in \mathcal{M}}{\operatorname{argmax}} (|R'(m')|). \quad (25)$$

E. Discussion on Algorithm and Complexity

Three operation processes incur additional computational complexity in the proposed method, i.e., normalized frequency offset estimation, parameter estimation, and interference cancelation. First of all, the normalized frequency estimation is required to carry out only one time when the system turns on. This is because, the ET does not usually change the operation frequency. In a time-invariant channel, the phase and power of interference signal can be considered to be almost constant within a frame. Once the receiver estimates the interfering signal parameters using the preamble, it can use them to detect subsequent symbols within the frame. Thus, the receiver performs parameter estimation once per data packet. Furthermore, for symbols after the preamble, we only need to detect the symbol given by (25) after canceling interference as in (24). The highest computational complexity of the proposed method is due to the normalized frequency offset estimation, which is given in (20). Since, we write $z(\varepsilon, n)$ as

$$\begin{aligned} z(\varepsilon, n) &= \frac{1}{\sqrt{2^S}} \sum_{k=0}^{2^S-1} \exp\left(j2\pi\left(\varepsilon k - \frac{k^2}{2^{S+1}} - \frac{n}{2^S}k\right)\right) \\ &= \frac{1}{\sqrt{2^S}} \sum_{k=0}^{2^S-1} \exp(j2\pi\varepsilon k) \exp\left(j2\pi\left(-\frac{k^2}{2^{S+1}} - \frac{n}{2^S}k\right)\right) \\ &= \frac{1}{\sqrt{2^S}} \sum_{k=0}^{2^S-1} \exp(j2\pi\varepsilon k) \cdot \kappa(k, n) \end{aligned} \quad (26)$$

where $\kappa(k, n)$ does not depends on unknown parameter ε , it can be prepared and stored in advance. Furthermore, the receiver needs to perform normalized frequency offset estimation only once when the system turns on as long as the ET does not change the carrier frequency for WPT. The required number of complex multiplications is shown in Table II.

V. SIMULATION RESULTS

In this section, we show the effectiveness of the proposed WPT interference cancelation method by the Monte Carlo simulation of 10^6 rounds using the C-based Julia language. The simulation parameters are listed in Table III. The LoRaWAN

TABLE III
SIMULATION PARAMETERS

Parameter	Value
Spreading Factor S	{7, 8, 9, 10}
Bandwidth W	125 [kHz]
SIR γ_{SIR}	{-5, -10, -15, -20} [dB]
Normalized frequency offset ε	{0.0, 0.1, ..., 0.5}
Preamble length N_{pr}	8
Payload length N_{pl}	20
Normalized Doppler frequency $f_{\text{D}}T_c$	10^{-6}

parameters are based on Japanese parameter configuration, i.e., AS923-MHz ISM Band [41], [42]. The bandwidth W is set to 125 [kHz]. The preamble length, N_{pr} , is set to the default value of 8 and the payload length, N_{pl} is set to 20. The normalized Doppler frequency, $f_{\text{D}}T_c$, is set to 10^{-6} where f_{D} denotes the maximum Doppler frequency and is assumed to be the pedestrian speed [43]. Since a LoRa transmitter and receiver are generally nomadic and signal bandwidth is narrow, it is general to consider AWGN channel or frequency-flat fading channel [13], [14], [15], [16], [17], [18], [22], [23], [24], [25], [26], [27], [28], [29]. However, we will also evaluate the performance of the proposed method under the multipath channel model in Section V-G. On the other hand, we assume that the channel between the ET and the LoRa receiver is a multipath fading channel, which is equivalently simulated by randomly generating the power and phase of the interfering WPT signal. In addition, we assume that uncoded system in this article, because we are interested in the cancelling performance of the proposed method.

A. Evaluation Criteria

1) *Symbol Error Rate*: A symbol error is defined as a difference between a transmitted symbol m and a symbol m^* detected by (25).

2) *Estimation Error of Interference Signal Parameter*: In the proposed interference rejection algorithm, first, it is necessary to estimate the normalized frequency offset ε , initial phase φ_{int} , and power P_{int} of the WPT interference signal. The estimation error of normalized frequency offset $\varepsilon_{\text{error}}$ is defined as

$$\varepsilon_{\text{error}} \triangleq \hat{\varepsilon} - \varepsilon. \quad (27)$$

Similarly, the phase estimation error φ_{error} from the estimated initial phase $\hat{\varphi}_{\text{int}}$ is defined as

$$\varphi_{\text{error}} \triangleq \hat{\varphi}_{\text{int}} - \varphi_{\text{int}}. \quad (28)$$

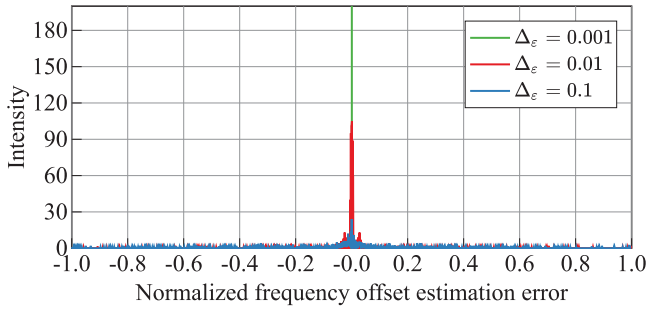


Fig. 8. Frequency offset estimation error ($S = 9$, $\gamma_{\text{SNR}} = -10$ [dB], and $\gamma_{\text{SIR}} = -10$ [dB].)

Define the normalized error $P_{\text{int,error}}$ with the estimated interfering signal power \hat{P}_{int} as

$$P_{\text{int,error}} \triangleq \frac{\hat{P}_{\text{int}} - P_{\text{int}}}{P_{\text{int}}}. \quad (29)$$

B. Distribution of Normalized Frequency Offset Estimation Error

This section evaluates the estimation accuracy of the normalized frequency offset obtained by (20) before the interference cancellation performance. Fig. 8 shows the distribution of estimation error of normalized frequency offset when true normalized frequency offset ε is randomly and uniformly generated within $[-0.5, 0.5]$ with step size of 10^{-3} . We set SNR $\gamma_{\text{SNR}} = -10$ [dB], SIR $\gamma_{\text{SIR}} = -10$ [dB], and $S = 9$. Search step size Δ_ε is set as a parameter. As Fig. 8 shows that the estimation error becomes significantly small as Δ_ε becomes small. In particular, in the case of $\Delta_\varepsilon = 0.001$, the estimation error is almost zero. This is because by considering phase offset $\psi^{\text{PF}}(\varepsilon', n)$ during projection, the correct frequency offset ε exhibits a large correlation value; otherwise, they show a significantly small value. There is a tradeoff between the estimation accuracy and computational complexity, as shown in Table II. However, as it is explained in Section IV, the receiver is required to perform normalized frequency offset estimation only once when the system turns on. Thus, the incurred computational complexity is not so high even if we set small Δ_ε . Fig. 9 shows the impact of frequency offset estimation on the SER performance of the proposed cancellation method. As the benchmark, the performances of the case with perfect knowledge of ε are also plotted. We can see from the figure that there is no performance degradation due to the frequency offset estimation error. We assume perfect normalized frequency offset estimation from the above in the following evaluation.

C. Performance With Perfect Preamble Detection and Synchronization

1) *SER Performance Under AWGN Channel*: We first assume an ideal preamble detection to evaluate the potential of the proposed interference cancellation method. In a practical scenario, a LoRa receiver first detects a preamble. Then, the receiver synchronizes the time and frequency to the LoRa signal and demodulates the payload [12], [24], [44]. The impact of the practical preamble detection on the performance will

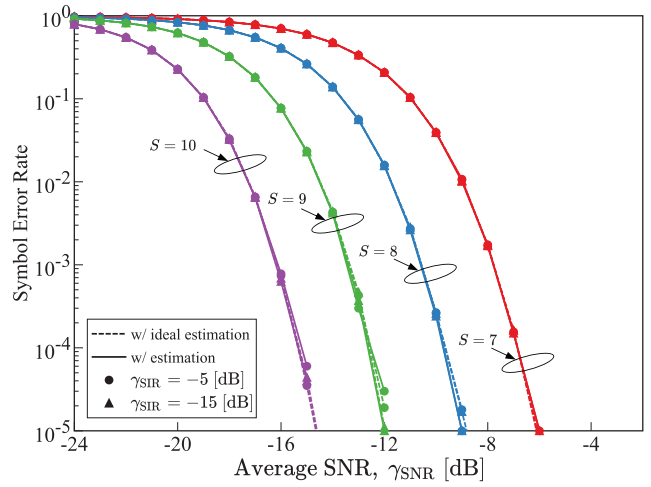


Fig. 9. Impact of frequency offset estimation error on SER performance.

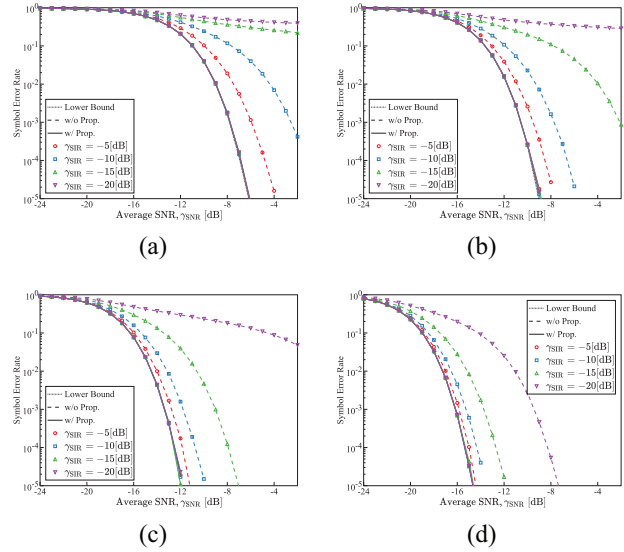


Fig. 10. Average SER of LoRa modulation under AWGN with WPT interference for $\varepsilon = 0$. (a) $S = 7$. (b) $S = 8$. (c) $S = 9$. (d) $S = 10$.

be evaluated in the subsequent section. Fig. 10 shows the SER performance with $\varepsilon = 0$ in AWGN channel. The dashed lines show the SER performances without WPT interference cancellation, and the solid lines show the SER performances with the proposed WPT interference cancellation method. We plot the ideal case with no WPT interference as a black dashed line for comparison. As can be seen from the figure, in the interference-free case, a larger SF provides better SER performance because of the processing gain. Also, as discussed in Section III-B, the WPT interference significantly degrades the SER. By increasing S , the de-chirping can effectively suppress the impact of WPT interference, resulting in better SER at the same SNR. On the other hand, the proposed WPT interference cancellation can significantly improve the SER performance irrespective of SF and achieve almost the same SER as the case without WPT interference.

Fig. 11 shows the impact of frequency offset ε on the SER performance. We set SIR γ_{SIR} to -5 [dB] and -10 [dB].

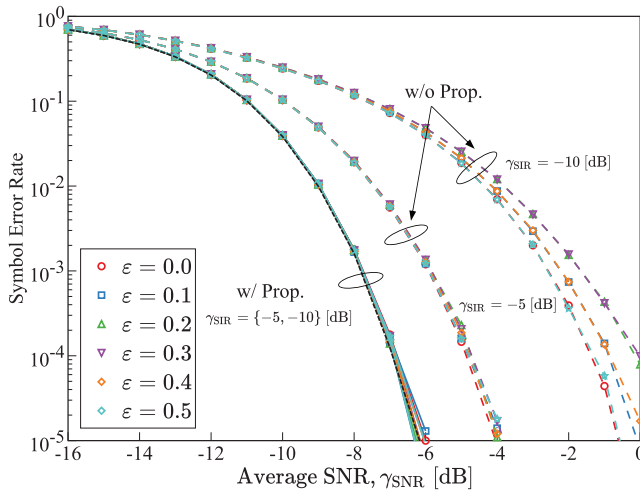


Fig. 11. Impact of frequency offset ϵ on SER performance in AWGN channel ($S = 7$).

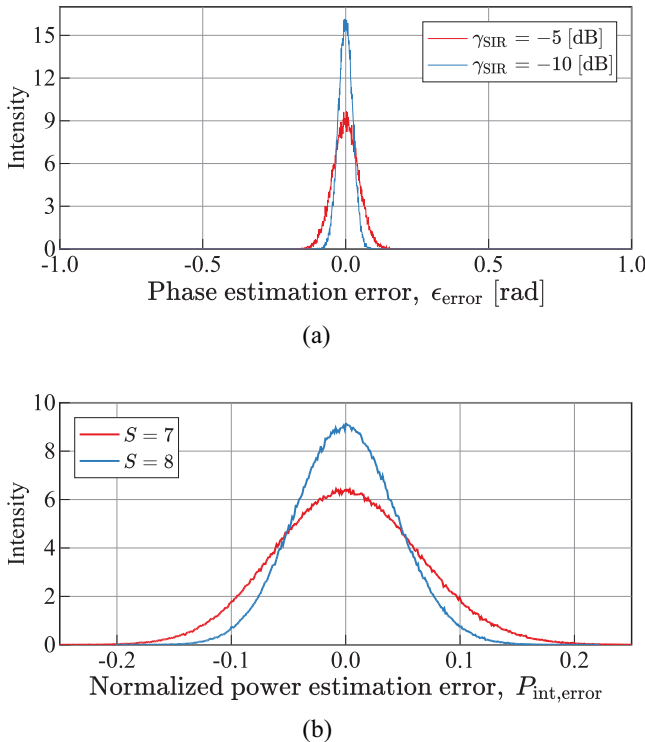


Fig. 12. Distribution of estimation error. (a) Phase estimation error ($S = 7$). (b) Power estimation error.

When $\gamma_{\text{SIR}} = -5$ [dB], the performance degradation is relatively small. On the other hand, when $\gamma_{\text{SIR}} = -10$ [dB], the SER performance significantly degrades if no WPT interference cancellation is introduced. The proposed WPT interference cancellation method can significantly improve the SER performance irrespective of ϵ and γ_{SIR} .

2) *Interference Signal Power and Phase Estimation Error:* Fig. 12(a) shows the distribution of the phase estimation error defined by (28) when $S = 7$, which shows that the proposed method can accurately estimate the initial phase φ_{int} . We observe that the estimation accuracy improves as the interfering signal becomes larger. This improvement is because

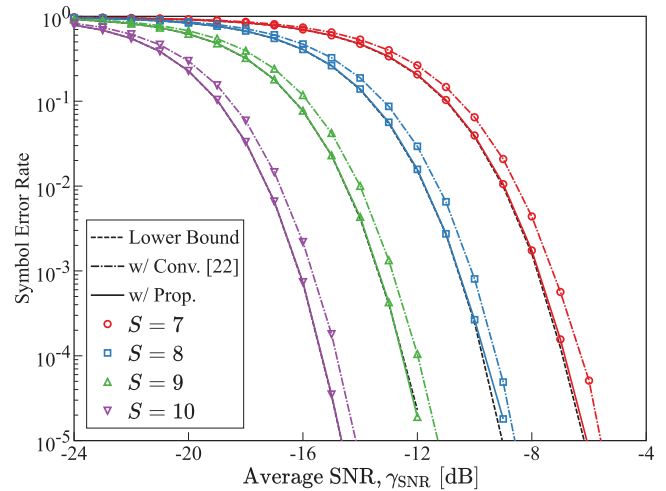


Fig. 13. Performance comparison against the conventional method [22].

the interference component becomes large relative to the noise component in each bin; hence, the interference component becomes dominant during the summation in (27). Fig. 12(b) shows the distribution of the interfering signal power estimation error defined by (29). The figure shows that the estimation accuracy improves as SF increases. Since the number of frequency bins to be summed up is $2^S - 1$, the number of noise components to be added increases, and the average sum converges to zero as SF increases. It can also be seen that the accuracy of both phase and power estimation depends on the variance of the noise. However, when the noise is strong, the system becomes a noise-limited system and interference from the WPT is not a major problem for performance degradation. (e.g., $S = 7$ and $\gamma_{\text{SNR}} = -12$ [dB]). On the other hand, under interference-limited conditions, the proposed method guarantees sufficient estimation accuracy.

3) *Comparison With Conventional Method:* Fig. 13 shows the SER performances of the proposed method and the interference suppression method by a frequency filter [22], where the suppression bandwidth is set to 12.5 [kHz] [22]. For the conventional method, we assume that carrier frequency of the WPT system f_c^{wpt} is ideally known. Fig. 13 shows that the conventional method can remove the WPT interference by the frequency filter. However, it also distorts the LoRa signal and degrades the SER performance. On the other hand, the proposed method efficiently removes the WPT interference and does not cause performance degradation.

D. Performance With Imperfect Preamble Detection and Synchronization

In this section, we evaluate the SER performance of the proposed WPT interference cancellation method with a practical preamble detection scheme. Fig. 14 shows the SER with preamble detection and synchronization. We have adopted the preamble detection and synchronization method proposed in [26]. When practical preamble detection and synchronization are adopted, the SER performance of the proposed method degrades compared to the ideal case. In particular, the proposed method cannot improve the SER performance

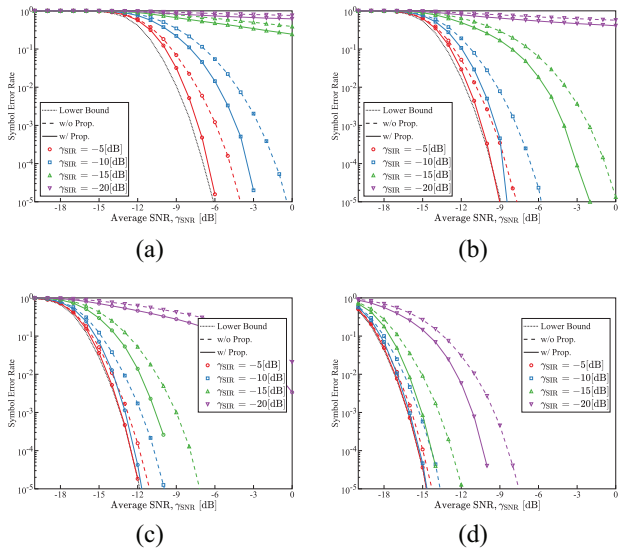


Fig. 14. Average SER performance of LoRa modulation under awgn and WPT interference considering preamble detection and synchronization. (a) $S = 7$. (b) $S = 8$. (c) $S = 9$. (d) $S = 10$.

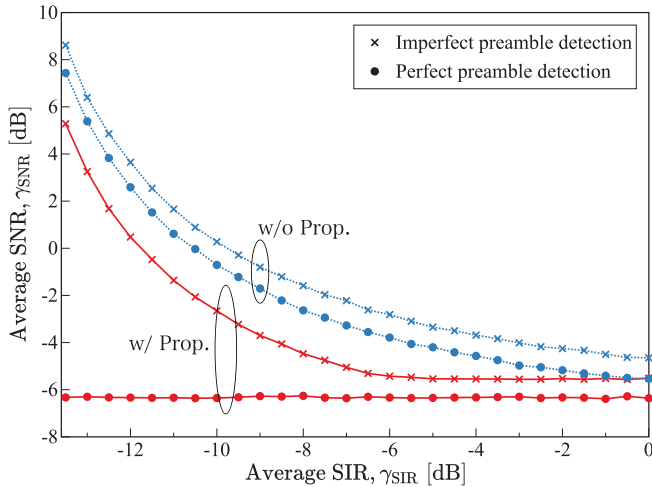


Fig. 15. Required SNR as a function of SIR to achieve target SER.

for $\gamma_{SIR} = \{-15, -20\}$ [dB]. This is because when WPT interference is present, the receiver fails to detect the preamble and misses the LoRa signal. Therefore, the LoRa receiver does not demodulate the subsequent symbols. Hence, we cannot expect any performance improvement. On the other hand, we can observe a performance improvement of up to 3 [dB] for $\gamma_{SIR} = \{-5, -10\}$ [dB]. This means that the chances of successful preamble detection are higher when the interference signal power is small. Then, the proposed method can utilize the preamble to estimate the phase and power of the interfering signal and can remove interference in subsequent symbols; thus, improving the SER performance.

E. Target SER Performance

Fig. 15 shows the required SNR for a target SER of 2×10^{-5} with $S = 7$ as a function of SIR values, in AWGN. The lines with circles show the case of ideal preamble detection and the lines with crossed lines show the case of imperfect preamble detection. As expected, without interference cancellation, the

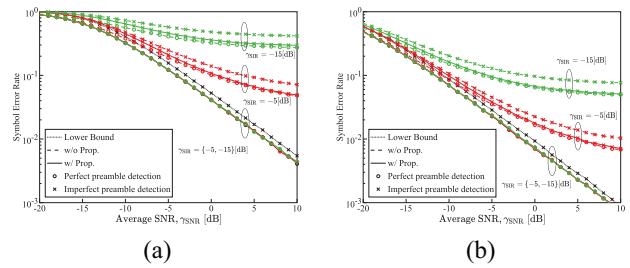


Fig. 16. Average SER performance of the LoRa modulation under Rayleigh fading with WPT interference for $\epsilon = 0$. (a) $S = 7$. (b) $S = 10$.

required SNR rapidly increases as SIR becomes small. On the other hand, the required SNR remains almost constant regardless of the SIR value when the proposed method is adopted. Note that the required SNR increases as SIR decreases whether or not the interference cancellation is adopted. This performance degradation is due to the preamble misdetection. However, the proposed interference cancellation method still can reduce the required SNR compared to the case without cancellation. The results also imply that the proposed method can be applied in different scenarios, if the requirements are met, i.e., if the region is above the red curve.

F. Symbol Error Rate Under Rayleigh Fading Channel

Fig. 16 shows the SER performance when $\epsilon = 0$ under the Rayleigh fading channel with and without considering preamble detection. In perfect preamble detection, it can be seen that the proposed WPT interference cancellation method can effectively remove the interference and improve the SER performance. On the other hand, in the case of imperfect preamble detection, the improvement is small. In particular, an error floor appears even when $SIR \gamma_{SIR} = -5$ [dB]. This is because LoRa signals with random phase due to the Rayleigh fading cancel each other out with WPT interference, resulting in preamble detection failure.

G. Symbol Error Rate Under Multipath Channel

Fig. 17 shows the SER performance of the proposed method when considering preamble detection in the 2-path channel environment with impulse response $g[k] = \sqrt{0.8}\delta(k) + \sqrt{0.2}\delta(k - 1)$ [7]. As can be seen from Fig. 17, the proposed method works well and achieves almost the same performance as the case without interference. This is because although the preamble signal propagated through the delayed paths are also added during summations of parameter estimation, they are very small compared to the added interference, and the multipath effect can be ignored.

VI. CONCLUSION

This article proposed a simple WPT interference cancellation method for LoRa receivers to take a step to move the coexistence of LoRaWAN and WPT systems further. The proposed method estimates the normalized frequency offset, phase, and power of interfering signals based on the frame preamble, then removes the interfering signal during the conventional LoRa demodulation. The computer simulation results showed

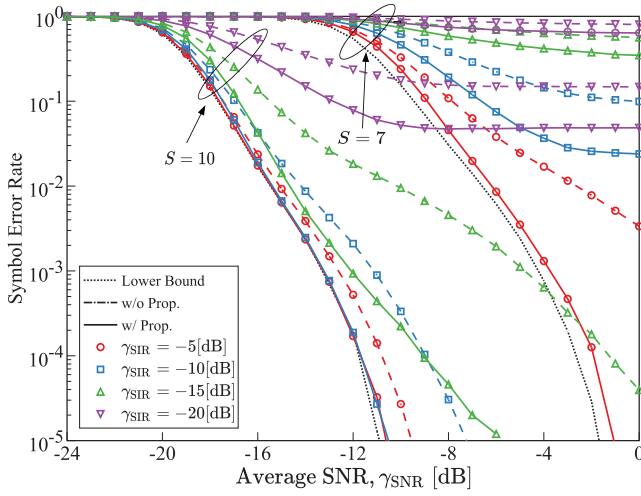


Fig. 17. Average SER performance under multipath channel environment.

that the proposed method could significantly improve the SER performance. Furthermore, it is shown that the proposed method can improve the SER performance by approximately 3 [dB] even when we consider practical preamble detection and synchronization. This article evaluated the case where a single WPT signal exists within the LoRa signal bandwidth. The interference cancellation method for multisine waveforms existing within the signal bandwidth is left as an important future study.

The main contribution of this article lies in the estimation and cancelation of the CW signal at the LoRa receiver, which does not require any modification at the transmitter side of both LoRa and WPT and their standards. That means, we can add the proposed method to the existing LoRaWAN systems. The proposed method has an advantage in the practical setup because the two different systems, i.e., LoRaWAN and WPT, can coexist with a slight modification of the LoRa receiver. The practical implementation of CSS-based modulation has been studied in several works of literature, such as [40] and [45]. Thus, the important future extension of this study is to implement the proposed method in a practical system and evaluate its performance in a real environment following the existing literature.

APPENDIX

Derivation follows [19], [33]. The DFT output of the LoRa signal propagating through multipath fading channel can be expressed as

$$\begin{aligned}
 R(n) &= \sum_{k=0}^{2^S-1} \{ (g[k] \otimes x[k]) x_0^*[k] \} \exp(-j2\pi \frac{n}{2^S} k) \\
 &= \sum_{k=0}^{2^S-1} \left\{ \left(\sum_{\ell=0}^{L^{\text{css}}-1} g_{\ell} x_{\bar{m}_{\ell}}[k - \tau_{\ell}^{\text{css}}] \right) x_0^*[k] \right\} \exp(-j2\pi \frac{n}{2^S} k) \\
 &= \sum_{\ell=0}^{L^{\text{css}}-1} g_{\ell} \left\{ \sum_{k=0}^{2^S-1} x_{\bar{m}_{\ell}}[k - \tau_{\ell}^{\text{css}}] x_0^*[k] \exp(-j2\pi \frac{n}{2^S} k) \right\}. \quad (30)
 \end{aligned}$$

Since the LoRa signal at each sampling point k depends on the relation between k and τ_{ℓ}^{css} , we consider the following different cases.

Case A: If $k > \tau_{\ell}^{\text{css}}$, i.e., $x_{\bar{m}_{\ell}}[k - \tau_{\ell}^{\text{css}}] = x_m[k - \tau_{\ell}^{\text{css}}]$.

1) If $0 \leq k - \tau_{\ell}^{\text{css}} \leq 2^S - m$

$$\begin{aligned}
 x_{\bar{m}_{\ell}}[k - \tau_{\ell}^{\text{css}}] &= x_m[k - \tau_{\ell}^{\text{css}}] \\
 &= \frac{1}{\sqrt{2^S}} \exp\left(j2\pi \frac{(k - \tau_{\ell}^{\text{css}} + m)^2}{2^{S+1}}\right). \quad (31)
 \end{aligned}$$

2) Otherwise

$$\begin{aligned}
 x_{\bar{m}_{\ell}}[k - \tau_{\ell}^{\text{css}}] &= x_m[k - \tau_{\ell}^{\text{css}}] \\
 &= \frac{1}{\sqrt{2^S}} \exp\left(j2\pi \frac{\left(\overbrace{k - \tau_{\ell}^{\text{css}} + m}^X - 2^S\right)^2}{2^{S+1}}\right) \\
 &= \frac{1}{\sqrt{2^S}} \exp\left(j2\pi \frac{X^2 - 2^{S+1}X + 2^{2S}}{2^{S+1}}\right) \\
 &= \frac{1}{\sqrt{2^S}} \exp\left(j2\pi \frac{X^2}{2^{S+1}}\right) \cdot \underbrace{\exp(-j2\pi(X + 2^{S-1}))}_1 \\
 &= \frac{1}{\sqrt{2^S}} \exp\left(j2\pi \frac{(k - \tau_{\ell}^{\text{css}} + m)^2}{2^{S+1}}\right). \quad (32)
 \end{aligned}$$

Case B: If $k \leq \tau_{\ell}^{\text{css}}$, i.e., $x_{\bar{m}_{\ell}}[k - \tau_{\ell}^{\text{css}}] = x_{\bar{m}}[2^S - \tau_{\ell}^{\text{css}} + k]$.

1) If $0 \leq k - \tau_{\ell}^{\text{css}} \leq 2^S - \bar{m}$

$$\begin{aligned}
 x_{\bar{m}_{\ell}}[k - \tau_{\ell}^{\text{css}}] &= x_{\bar{m}}[2^S - \tau_{\ell}^{\text{css}} + k] \\
 &= \frac{1}{\sqrt{2^S}} \exp\left(j2\pi \frac{\left(2^S + \overbrace{(\bar{m} - \tau_{\ell}^{\text{css}} + k)}^Y\right)^2}{2^{S+1}}\right) \\
 &= \frac{1}{\sqrt{2^S}} \exp\left(j2\pi \frac{Y^2 - 2^{S+1}Y + 2^{2S}}{2^{S+1}}\right) \\
 &= \frac{1}{\sqrt{2^S}} \exp\left(j2\pi \frac{Y^2}{2^{S+1}}\right) \cdot \underbrace{\exp(-j2\pi(Y + 2^{S-1}))}_1 \\
 &= \frac{1}{\sqrt{2^S}} \exp\left(j2\pi \frac{(k - \tau_{\ell}^{\text{css}} + \bar{m})^2}{2^{S+1}}\right). \quad (33)
 \end{aligned}$$

2) Otherwise

$$\begin{aligned}
 x_{\bar{m}_{\ell}}[k - \tau_{\ell}^{\text{css}}] &= x_{\bar{m}}[2^S - \tau_{\ell}^{\text{css}} + k] \\
 &= \frac{1}{\sqrt{2^S}} \exp\left(j2\pi \frac{(2^S - \tau_{\ell}^{\text{css}} + k + \bar{m} - 2^S)^2}{2^{S+1}}\right) \\
 &= \frac{1}{\sqrt{2^S}} \exp\left(j2\pi \frac{(k - \tau_{\ell}^{\text{css}} + \bar{m})^2}{2^{S+1}}\right). \quad (34)
 \end{aligned}$$

From (31) to (34), $x_{\bar{m}_{\ell}}[k - \tau_{\ell}^{\text{css}}]$ can be expressed as

$$x_{\bar{m}_{\ell}}[k - \tau_{\ell}^{\text{css}}] = \frac{1}{\sqrt{2^S}} \exp\left(j2\pi \frac{(k - \tau_{\ell}^{\text{css}} + \bar{m})^2}{2^{S+1}}\right). \quad (35)$$

Thus, multiplying the downchirp $x_0^*[k]$ yields

$$\begin{aligned} x_{\tilde{m}_\ell}[k - \tau_\ell^{\text{css}}]x_0^*[k] &= \frac{1}{2^S} \exp\left(j2\pi \frac{(m - \tau_\ell^{\text{css}})^2}{2^{S+1}}\right) \cdot \exp\left(j2\pi \frac{k(m - \tau_\ell^{\text{css}})}{2^S}\right). \end{aligned} \quad (36)$$

Thus, (30) can be simplified as

$$\begin{aligned} &\sum_{\ell=0}^{L^{\text{css}}-1} g_\ell \left\{ \sum_{k=0}^{2^S-1} x_{\tilde{m}_\ell}[k - \tau_\ell^{\text{css}}]x_0^*[k] \exp\left(-j2\pi \frac{n}{2^S}k\right) \right\} \\ &= \sum_{\ell=0}^{L^{\text{css}}-1} g_\ell \left\{ \sum_{k=0}^{2^S-1} \frac{1}{2^S} \exp\left(j2\pi \frac{(\tilde{m}_\ell - \tau_\ell^{\text{css}})^2}{2^{S+1}}\right) \right. \\ &\quad \times \left. \exp\left(j2\pi \frac{k(\tilde{m}_\ell - \tau_\ell^{\text{css}})}{2^S}\right) \exp\left(-j2\pi \frac{n}{2^S}k\right) \right\} \\ &= \sum_{\ell=0}^{L^{\text{css}}-1} g_\ell \underbrace{\exp\left(j2\pi \frac{(\tilde{m}_\ell - \tau_\ell^{\text{css}})^2}{2^{S+1}}\right)}_{\triangleq \tilde{g}_{\tilde{m}_\ell}(\tau_\ell^{\text{css}})} \\ &\quad \times \left\{ \frac{1}{2^S} \sum_{k=0}^{2^S-1} \exp\left(j2\pi \frac{\tilde{m}_\ell - \tau_\ell^{\text{css}} - n}{2^S}k\right) \right\} \\ &= \sum_{\ell=0}^{L^{\text{css}}-1} \tilde{g}_{\tilde{m}_\ell}(\tau_\ell^{\text{css}}) \left\{ \frac{1}{2^S} \sum_{k=0}^{2^S-1} \exp\left(j2\pi \frac{\tilde{m}_\ell - \tau_\ell^{\text{css}} - n}{2^S}k\right) \right\}. \end{aligned} \quad (37)$$

REFERENCES

- [1] A. Zanella, N. Bui, A. Castellani, L. Vangelista, and M. Zorzi, "Internet of Things for smart cities," *IEEE Internet Things J.*, vol. 1, no. 1, pp. 22–32, Feb. 2014.
- [2] H. I. Kobo, A. M. Abu-Mahfouz, and G. P. Hancke, "A survey on software-defined wireless sensor networks: Challenges and design requirements," *IEEE Access*, vol. 5, pp. 1872–1899, 2017.
- [3] U. Raza, P. Kulkarni, and M. Sooriyabandara, "Low power wide area networks: An overview," *IEEE Commun. Surveys Tuts.*, vol. 19, no. 2, pp. 855–873, 2nd Quart., 2017.
- [4] O. Georgiou and U. Raza, "Low power wide area network analysis: Can LoRa scale?" *IEEE Wireless Commun. Lett.*, vol. 6, no. 2, pp. 162–165, Apr. 2017.
- [5] A. Lavric, A. I. Petrariu, and V. Popa, "SigFox communication protocol: The new era of IoT?" in *Proc. Int. Conf. Sens. Instrum. IoT Era (ISSI)*, Aug. 2019, pp. 1–4.
- [6] M. Chen, Y. Miao, Y. Hao, and K. Hwang, "Narrow band Internet of Things," *IEEE Access*, vol. 5, pp. 20557–20577, 2017.
- [7] L. Vangelista, "Frequency shift chirp modulation: The LoRa modulation," *IEEE Signal Process. Lett.*, vol. 24, no. 12, pp. 1818–1821, Dec. 2017.
- [8] J. Haxhibeqiri, E. De Poorter, I. Moerman, and J. Hoebeke, "A survey of LoRaWAN for IoT: From technology to application," *Sensors*, vol. 18, no. 11, p. 3995, Nov. 2018.
- [9] Z. Zhang, H. Pang, A. Georgiadis, and C. Cecati, "Wireless power transfer—An overview," *IEEE Trans. Ind. Electron.*, vol. 66, no. 2, pp. 1044–1058, Feb. 2019.
- [10] S. Bi, C. K. Ho, and R. Zhang, "Wireless powered communication: Opportunities and challenges," *IEEE Commun. Mag.*, vol. 53, no. 4, pp. 117–125, Apr. 2015.
- [11] Y. Chen, D. B. da Costa, and H. Ding, "Interference analysis in wireless power transfer," *IEEE Commun. Lett.*, vol. 21, no. 10, pp. 2318–2321, Oct. 2017.
- [12] "LoRaWAN specification v1.1." Feb. 2021. [Online]. Available: <https://lora-alliance.org/resource-hub/lorawan-specification-v1-1>
- [13] T. Elshabrawy and J. Robert, "Closed-form approximation of LoRa modulation BER performance," *IEEE Commun. Lett.*, vol. 22, no. 9, pp. 1778–1781, Sep. 2018.
- [14] A. Marquet, N. Montavont, and G. Z. Papadopoulos, "Towards an SDR implementation of LoRa: Reverse-engineering demodulation strategies and assessment over Rayleigh channel," *Comput. Commun.*, vol. 153, pp. 595–605, Mar. 2020.
- [15] B. Dunlop, H. H. Nguyen, R. Barton, and J. Henry, "Interference analysis for LoRa chirp spread spectrum signals," in *Proc. IEEE Can. Conf. Electr. Comput. Eng. (CCECE)*, 2019, pp. 1–5.
- [16] O. Afisiadis, M. Cotting, A. Burg, and A. Balatsoukas-Stimming, "On the error rate of the LoRa modulation with interference," *IEEE Trans. Wireless Commun.*, vol. 19, no. 2, pp. 1292–1304, Feb. 2020.
- [17] T. Elshabrawy and J. Robert, "Analysis of BER and coverage performance of LoRa modulation under same spreading factor interference," in *Proc. IEEE 29th Annu. Int. Symp. Pers. Indoor Mobile Radio Commun. (PIMRC)*, Sep. 2018, pp. 1–6.
- [18] D. Croce, M. Gucciardo, S. Mangione, G. Santaromita, and I. Tinnirello, "Impact of LoRa imperfect orthogonality: Analysis of link-level performance," *IEEE Commun. Lett.*, vol. 22, no. 4, pp. 796–799, Apr. 2018.
- [19] C. Demeslay, P. Rostaing, and R. Gautier, "Theoretical performance of LoRa system in multipath and interference channels," *IEEE Internet Things J.*, vol. 9, no. 9, pp. 6830–6843, May 2022.
- [20] C. Orfanidis, L. M. Feeney, M. Jacobsson, and P. Gunningberg, "Investigating interference between LoRa and IEEE 802.15.4g networks," in *Proc. IEEE Int. Conf. Wireless Mobile Comput. Netw. Commun. (WiMob)*, Oct. 2017, pp. 1–8.
- [21] J. Haxhibeqiri et al., "Sub-gigahertz inter-technology interference. How harmful is it for LoRa?" in *Proc. IEEE Int. Smart Cities Conf. (ISC2)*, Sep. 2018, pp. 1–7.
- [22] T. Elshabrawy and J. Robert, "The impact of ISM interference on LoRa BER performance," in *Proc. IEEE Global Conf. Internet Things (GCIoT)*, Jan. 2019, pp. 1–5.
- [23] O. Afisiadis, S. Li, J. Tapparel, A. Burg, and A. Balatsoukas-Stimming, "On the advantage of coherent LoRa detection in the presence of interference," *IEEE Internet Things J.*, vol. 8, no. 14, pp. 11581–11593, Jul. 2021.
- [24] A. A. Tesfay, E. P. Simon, G. Ferré, and L. Clavier, "Serial interference cancellation for improving uplink in LoRa-like networks," in *Proc. IEEE 31st Annu. Int. Symp. Pers. Indoor Mobile Radio Commun. (PIMRC)*, 2020, pp. 1–6.
- [25] M. A. B. Temim, G. Ferré, B. Laporte-Fauret, D. Dallet, B. Minger, and L. Fuché, "An enhanced receiver to decode superposed LoRa-like signals," *IEEE Internet Things J.*, vol. 7, no. 8, pp. 7419–7431, Aug. 2020.
- [26] D. Garlisi, S. Mangione, F. Giuliano, D. Croce, G. Garbo, and I. Tinnirello, "Interference cancellation for LoRa gateways and impact on network capacity," *IEEE Access*, vol. 9, pp. 128133–128146, 2021.
- [27] X. Xia, Y. Zheng, and T. Gu, "FTrack: Parallel decoding for LoRa transmissions," *IEEE/ACM Trans. Netw.*, vol. 28, no. 6, pp. 2573–2586, Dec. 2020.
- [28] Z. Xu, P. Xie, and J. Wang, "Pyramid: Real-time LoRa collision decoding with peak tracking," in *Proc. IEEE Conf. Comput. Commun.*, May 2021, pp. 1–9.
- [29] B. Hu, Z. Yin, S. Wang, Z. Xu, and T. He, "SCLoRa: Leveraging multi-dimensionality in decoding collided LoRa transmissions," in *Proc. IEEE 28th Int. Conf. Netw. Protocols*, Oct. 2020, pp. 1–11.
- [30] A. Ovechkin, T. Claeys, D. Vanoost, G. A. E. Vandenbosch, and D. Pissort, "A novel method of removing the influence of continuous electromagnetic wave disturbances in OFDM systems," *IEEE Trans. Electromagn. Compat.*, vol. 64, no. 2, pp. 338–347, Apr. 2022.
- [31] S. M. Danish, H. K. Qureshi, S. Jangsher, and M. Lestas, "Effects of wireless power transfer on LoRaWAN join procedure," in *Proc. 14th Int. Wireless Commun. Mobile Comput. Conf. (IWCMC)*, Jun. 2018, pp. 944–949.
- [32] X. Liu, Y. Xue, and H. Sun, "Analog domain self-interference cancellation method based on digital aided processing," in *Proc. IEEE 9th Joint Int. Inf. Technol. Artif. Intell. Conf. (ITAIC)*, Dec. 2020, pp. 1256–1260.
- [33] T. Elshabrawy and J. Robert, "Interleaved chirp spreading LoRa-based modulation," *IEEE Internet Things J.*, vol. 6, no. 2, pp. 3855–3863, Apr. 2019.
- [34] I. B. F. de Almeida, M. Chafii, A. Nimr, and G. Fettweis, "Alternative chirp spread spectrum techniques for LPWANs," *IEEE Trans. Green Commun. Netw.*, vol. 5, no. 4, pp. 1846–1855, Dec. 2021.
- [35] B. Clerckx, K. Huang, L. R. Varshney, S. Ulukus, and M.-S. Alouini, "Wireless power transfer for future networks: Signal processing, machine learning, computing, and sensing," *IEEE J. Sel. Top. Signal Process.*, vol. 15, no. 5, pp. 1060–1094, Aug. 2021.

- [36] B. Clerckx and E. Bayguzina, "Low-complexity adaptive multisine waveform design for wireless power transfer," *IEEE Antennas Wireless Propag. Lett.*, vol. 16, pp. 2207–2210, 2017.
- [37] A. Boaventura, D. Belo, R. Fernandes, A. Collado, A. Georgiadis, and N. B. Carvalho, "Boosting the efficiency: Unconventional waveform design for efficient wireless power transfer," *IEEE Microw. Mag.*, vol. 16, no. 3, pp. 87–96, Apr. 2015.
- [38] A. J. S. Boaventura, A. Collado, A. Georgiadis, and N. B. Carvalho, "Spatial power combining of multi-sine signals for wireless power transmission applications," *IEEE Trans. Microw. Theory Techn.*, vol. 62, no. 4, pp. 1022–1030, Apr. 2014.
- [39] S. Abeywickrama, R. Zhang, and C. Yuen, "Refined nonlinear rectenna modeling and optimal waveform design for multi-user multi-antenna wireless power transfer," *IEEE J. Sel. Top. Signal Process.*, vol. 15, no. 15, pp. 1198–1210, Aug. 2021.
- [40] J. C. Liando, A. Gamage, A. W. Tengourtius, and M. Li, "Known and unknown facts of LoRa: Experiences from a large-scale measurement study," *ACM Trans. Sens. Netw.*, vol. 15, no. 2, pp. 1–35, Feb. 2019.
- [41] "RP2-1.0.1 LoRaWAN regional parameters." LoRa Alliance Technical Committee. 2020. [Online]. Available: <https://lora-alliance.org/resource-hub/rp2-101-lorawan-regional-parameters/>
- [42] "Semtech SX1272/73 LoRa transceiver." 2023. [Online]. Available: <https://www.semtech.com/products/wireless-rf/lora-core/sx1272>
- [43] W. Xu, J. Y. Kim, W. Huang, S. S. Kanhere, S. K. Jha, and W. Hu, "Measurement, characterization, and modeling of LoRa technology in multifloor buildings," *IEEE Internet Things J.*, vol. 7, no. 1, pp. 298–310, Jan. 2020.
- [44] C. Bernier, F. Dehmas, and N. Deparis, "Low complexity LoRa frame synchronization for ultra-low power software-defined radios," *IEEE Trans. Commun.*, vol. 68, no. 5, pp. 3140–3152, May 2020.
- [45] D. Belo et al., "IQ impedance modulator front-end for low-power LoRa backscattering devices," *IEEE Trans. Microw. Theory Techn.*, vol. 67, no. 12, pp. 5307–5314, Dec. 2019.



Ryota Kumada received the B.E. degree in information and communication engineering from The University of Electro-Communications, Chofu, Japan, in 2021, where he is currently pursuing the M.E. degree.

His research interests include LPWA network.



Koichi Adachi (Senior Member, IEEE) received the B.E., M.E., and Ph.D. degrees in engineering from Keio University, Tokyo, Japan, in 2005, 2007, and 2009 respectively.

He was the Visiting Researcher with the City University of Hong Kong, Hong Kong, in April 2009 and the Visiting Research Fellow with the University of Kent, Canterbury, U.K., from June to August 2009. From May 2010 to May 2016, he was with the Institute for Infocomm Research, A*STAR, Singapore. He is currently an Associate Professor

with The University of Electro-Communications, Chofu, Japan. His research interests include cooperative communications and energy-efficient communication technologies.

Dr. Adachi was awarded the Excellent Editor Award from IEEE ComSoc MMTC in 2013. He is a coauthor of the WPMC2020 Best Student Paper Award. He served as a General Co-Chair for the 10th and 11th IEEE Vehicular Technology Society Asia-Pacific Wireless Communications Symposium, a Track Co-Chair for Transmission Technologies and Communication Theory of the 78th and 80th IEEE Vehicular Technology Conference in 2013 and 2014, respectively, and a Symposium Co-Chair for Communication Theory Symposium of IEEE Globecom 2018, a Tutorial Co-Chair for IEEE ICC 2019, and a Symposium Co-Chair for Wireless Communications Symposium of IEEE Globecom 2020. He was an Associate Editor of *IET Transactions on Communications* from 2015 to 2017, IEEE WIRELESS COMMUNICATIONS LETTERS from 2016 to 2022, IEEE TRANSACTIONS ON VEHICULAR TECHNOLOGY from 2016 to 2018, IEEE TRANSACTIONS ON GREEN COMMUNICATIONS AND NETWORKING from 2016 to 2022, and IEEE OPEN JOURNAL OF VEHICULAR TECHNOLOGY since 2019. He was recognized as the Exemplary Reviewer from IEEE WIRELESS COMMUNICATIONS LETTERS in 2012, 2013, 2014, and 2015. From 2007 to 2010, he was a Japan Society for the Promotion of Science Research Fellow. He is a member of the IEICE.